doi: 10.1111/j.1460-2695.2005.00919.x

Cohesive-zone modelling of the deformation and fracture of spot-welded joints

M. N. CAVALLI[1], M. D. THOULESS[2,3] and Q. D. YANG[4]

[1] *Department of Mechanical Engineering, University of North Dakota, Grand Forks, ND 58202-8359;* [2] *Department of Mechanical Engineering,* [3] *Department of Materials Science and Engineering, University of Michigan, Ann Arbor, MI, and* [4] *Rockwell Scientific Company, Thousand Oaks, CA, USA*

Received in final form 2 April 2005

ABSTRACT The deformation and failure of spot-welded joints have been successfully modelled using a cohesive-zone model for fracture. This has been accomplished by implementing a user-defined, three-dimensional, cohesive-zone element within a commercial finite-element package. The model requires two material parameters for each mode of deformation. Results show that the material parameters from this type of approach are transferable for identical spot welds in different geometries where a single parameter (such as maximum stress) is not. The approach has been demonstrated using a model system consisting of spot-welded joints made from 5754 aluminium sheets. The techniques for determining the cohesive fracture parameters for both nugget fracture and nugget pullout are described in this paper. It has been demonstrated that once the appropriate cohesive parameters for a weld are determined, quantitative predictions can be developed for the strengths, deformations and failure mechanisms of different geometries with nominally identical welds.

Keywords cohesive-zone modelling; finite element modelling; fracture; resistance spot-welding.

NOMENCLATURE

G = shear modulus
Γ_{IN} = mode-I nugget fracture toughness
Γ_{IIN} = mode-II nugget fracture toughness
Γ_{IIIN} = mode-III nugget fracture toughness
Γ_{IP} = mode-I pullout fracture toughness
Γ_{IIP} = mode-II pullout fracture toughness
Γ_{IIIP} = mode-III pullout fracture toughness
$\mathcal{G}_{\mathrm{I}}$ = mode-I energy release rate
$\mathcal{G}_{\mathrm{II}}$ = mode-II energy release rate
$\mathcal{G}_{\mathrm{III}}$ = mode-III energy release rate
E = Young's modulus
$\widehat{\sigma}_{\mathrm{N}}$ = mode-I nugget cohesive strength
$\widehat{\tau}_{\mathrm{N}}$ = mode-II (and III) nugget cohesive strength
$\widehat{\sigma}_{\mathrm{P}}$ = mode-I pullout cohesive strength
$\widehat{\tau}_{\mathrm{P}}$ = mode-II (and III) pullout cohesive strength

INTRODUCTION

Structural joints between thin metal sheets are crucial components of many engineering designs. Methods of joining metal sheets include clamping them together with bolts or rivets, chemically bonding them with an intermediate layer such as an adhesive, or welding them together. Resistance spot-welding, which makes use of the contact resistance between metal parts to induce localized melting when an electric current is applied, is widely used in the

Correspondence: M. N. Cavalli. E-mail: matthewcavalli@mail.und.nodak.edu

automotive industry. A complete understanding of how to analyse the deformation and fracture of spot-welded joints, and how to use this analysis to make predictions about their performance, would greatly enhance the efficient design of safe automotive structures.

One method of analysing spot-welded joints is to calculate the stress distribution, and to determine the regions where the stresses are elevated.[1–3] However, while the knowledge of the locations of the highest stresses can help predict *where* a spot-welded structure is likely to fracture, it cannot, by itself, predict the *load at which* failure will occur. Such predictions require both suitable failure criteria and a method for implementing these criteria into numerical calculations. Existing failure criteria for spot-welded joints generally share the starting assumption that a single parameter (e.g. a critical stress or force) characterizes the failure of a spot weld that is subjected to a pure state of stress (e.g. shear or tension). In other words, there is an implicit assumption that it is possible to use a single strength parameter as the sole failure criterion under simple loading conditions. For example, Lee *et al.*[4] and Lin *et al.*[5] based their failure criterion on the average tensile and shear strengths of a weld. Wung and co-authors[6,7] developed a similar criterion introducing a bending moment and a torque as two additional modes of loading a weld.

These strength-based approaches for predicting the performance of a weld appear to work quite well if the geometry of the joint is kept fairly constant. Substantial changes in the geometry may change the relative stress levels in different regions of the weld, fundamentally affecting the average stress at which failure occurs. This is a classic issue in fracture, and it is well established that energy-based failure criteria need to be included in any quantitative fracture analysis. However, the use of only energy-based failure criteria is not appropriate unless the scale of plastic deformation in a structure is much less than any characteristic length. Owing to large-scale plasticity that accompanies fracture, this condition is generally violated with any spot-welded sheet metal. Fracture problems in which plastic deformation is significant can be analysed by the use of cohesive-zone models that incorporate both strength and energy criteria for fracture.[8–16] This paper provides the first example of using cohesive-zone model for analysing welded structures, demonstrating an experimental determination of the cohesive parameters and their use in predicting the strength of joints.

The approach developed for this paper is a direct extension of earlier work on adhesive joints.[8–11] Standard finite-element methods are used to model the deformation of the adherends. Bonding across any potential rupture plane is represented by a cohesive law that is characterized by two parameters: a cohesive strength and a fracture energy. Relative displacement of the rupture planes is resisted by the cohesive stresses. Fracture occurs when a critical relative displacement (corresponding to the critical fracture energy) is reached.

The earlier work on adhesive joints was successful in part because of the significant numerical simplifications that resulted from not attempting to model the details of the adhesive. The role of the adhesive in the analysis was reduced to one of merely providing tractions across the interface. These tractions characterized the deformation of the adhesive layer up to failure. A similar simplification for welds is adopted in the present work. For example, the weld nugget is not explicitly modelled in the analysis; it is replaced by a cohesive law acting on the appropriate region of the adherends. The cohesive parameters for the nugget and other failure planes are determined by comparing experimental observations of strength and deformation to numerical predictions using a mixed-mode failure criterion to link the normal and shear modes of deformation (mode-I, -II and -III). After obtaining values for the cohesive parameters, verification of the modelling is done by comparing numerical predictions based on these parameters to experimental results for other geometries.

It should be emphasized that it is not the purpose of this work to do process modelling. The cohesive parameters of welds produced under nominally similar conditions are assumed not to be significantly affected by changes in the geometry of a joint. The major intent of this work is to investigate whether cohesive-zone models can be used to characterize welds formed under reasonably similar conditions, and whether the cohesive parameters can then be used to predict the performance of different joints made from approximately similar welds. Once these concepts have been established, it should subsequently be possible to use the methodology to predict how changes in the properties of a weld will affect the performance of a joint and, perhaps, incorporate this into a process-modelling program.

NUMERICAL MODELLING

Two particular mechanisms of weld failure are considered in this paper. These are rupture of the nugget itself, and failure of the adherend around the circumference of the nugget resulting in weld pullout. Any numerical model must incorporate both failure conditions, and be able to predict transitions between them. It should further be noted that three possible modes of deformation, mode-I, -II and -III (normal and two shear modes), may be associated with each of the failure mechanisms. As discussed above, two cohesive-zone parameters need to be defined for each mode of each mechanism: The maximum stress that each rupture plane can support (the normal and shear cohesive strengths), and the energy directly associated with fracturing each rupture plane in the appropriate mode (the mode-I, -II and -III toughness).

Table 1 Cohesive-zone parameters used in the numerical modelling of the spot-welded joint

	Mode-I		Mode-II	
	Strength (MPa)	Toughness (kJm^{-2})	Strength (MPa)	Toughness (kJm^{-2})
Nugget fracture	$\hat{\sigma}_N = 290 \pm 30$	$\Gamma_{IN} = 13 \pm 2$	$\hat{\tau}_N = 200 \pm 20$	$\Gamma_{IIN} = 26 \pm 4$
Weld pullout	$\hat{\sigma}_P = 340 \pm 10$	$\Gamma_{IP} = 13 \pm 2$	$\hat{\tau}_P = 230 \pm 10$	$\Gamma_{IIP} = 26 \pm 4$

Therefore, in principle, 12 independent fracture parameters need to be determined for a weld—a strength and toughness for each of the three modes by which the nugget can fail, and a strength and toughness for each of the three modes associated with pullout. However, owing to the inherent symmetry of the user element, and to reduce the required number of fracture parameters, it was assumed that mode-II and -III have identical fracture parameters for each mechanism. This reduced to eight the number of cohesive-zone parameters that need to be determined: the cohesive strengths and toughness for nugget failure; and the cohesive strengths and toughness for pullout failure (Table 1). Simple trapezoidal traction-separation laws were used in this work, as shown in Fig. 1. The shapes of these curves were chosen to be similar for every failure mode, but with different values of peak stress and toughness. The inherent assumption in using these laws, that the shape of the cohesive law is of secondary importance when modelling fracture,[14,15] was verified by calculations with slightly different forms of the cohesive laws. However, while the precise details of the fracture process do not need to be modelled (beyond capturing the characteristic toughness and cohesive strength), at some level the shape shown in Fig. 1 can be considered as a stylistic representation of elastic–perfectly plastic deformation.

The traction-separation laws were incorporated into a commercial 3-D finite-element code (ABAQUS versions 5.8.16 and 6.3) through the use of eight-noded, user-defined brick elements. The elements deformed according to the traction-separation law appropriate for the region of material and for the mode of deformation. The thickness of the elements was set at 0.25 mm, and the initial slopes of the traction-separation laws (Fig. 1) were adjusted so that they were numerically equal to E or G, as appropriate, when the displacements were normalized by the element thickness. Systematic investigations of numerical issues, such as mesh refinement, ensured that the results were accurate within any uncertainty limits given. Details of the code and some additional numerical considerations are given in the accompanying Ph.D. thesis.[17] When doing a full failure analysis, cohesive elements were placed in any region where failure was expected. For example, the nugget between the two adherends was completely replaced by the cohesive elements to allow nugget failure. Similarly, a ring of the cohesive elements was placed through the full thickness of the adherend around the circumference of the nugget to allow nugget pullout. For loading in a single mode of deformation, failure occurred when the displacement between two nodes in a node pair reached the critical value δ_c (i.e. when the complete traction-separation law had been traced). At this point, the relevant node pair lost all load-bearing capability, and an increment of rupture occurred. In other words, failure occurred when the energy-release rate reached the toughness appropriate for that mode. A simple mixed-mode failure criterion of the form[11]

$$\frac{\mathcal{G}_I}{\Gamma_I} + \frac{\mathcal{G}_{II}}{\Gamma_{II}} + \frac{\mathcal{G}_{III}}{\Gamma_{III}} = 1 \tag{1}$$

was assumed.[a] After every loading increment, Eq. (1) was assessed for each node pair of every cohesive-zone element in the model. Any node pair that met this criterion was deemed to have failed, and it was no longer capable of supporting load. This represented an increment of crack advance through the material. The analysis was then repeated for this new condition with a failed node pair, and the loading continued.

DETERMINATION OF MATERIAL AND COHESIVE-ZONE PARAMETERS

Material parameters

The goals of the experimental portion of this study were to determine the required parameters, and to confirm that the approach could be used to predict the behaviour of spot-welded joints. To do this, it was essential to model the properties of the adherends and heat-affected zone[18] correctly. The metal used in this study was 5754-O aluminium because, as with other 5000-series aluminium alloys, it is a non-heat-treatable alloy[19] and, hence, was expected to minimize the potential variability of the material properties in the heat-affected zone.

Residual stresses in spot-welded joints arise from three sources: plasticity induced by the indentation action of the electrode tips;[20] plasticity induced by deformation of a joint into the desired shape before testing or service; and

[a]Note that while Γ_{II} and Γ_{III} were assumed to be identical in this paper, $\mathcal{G}_{II}$ and $\mathcal{G}_{III}$ will generally be different.

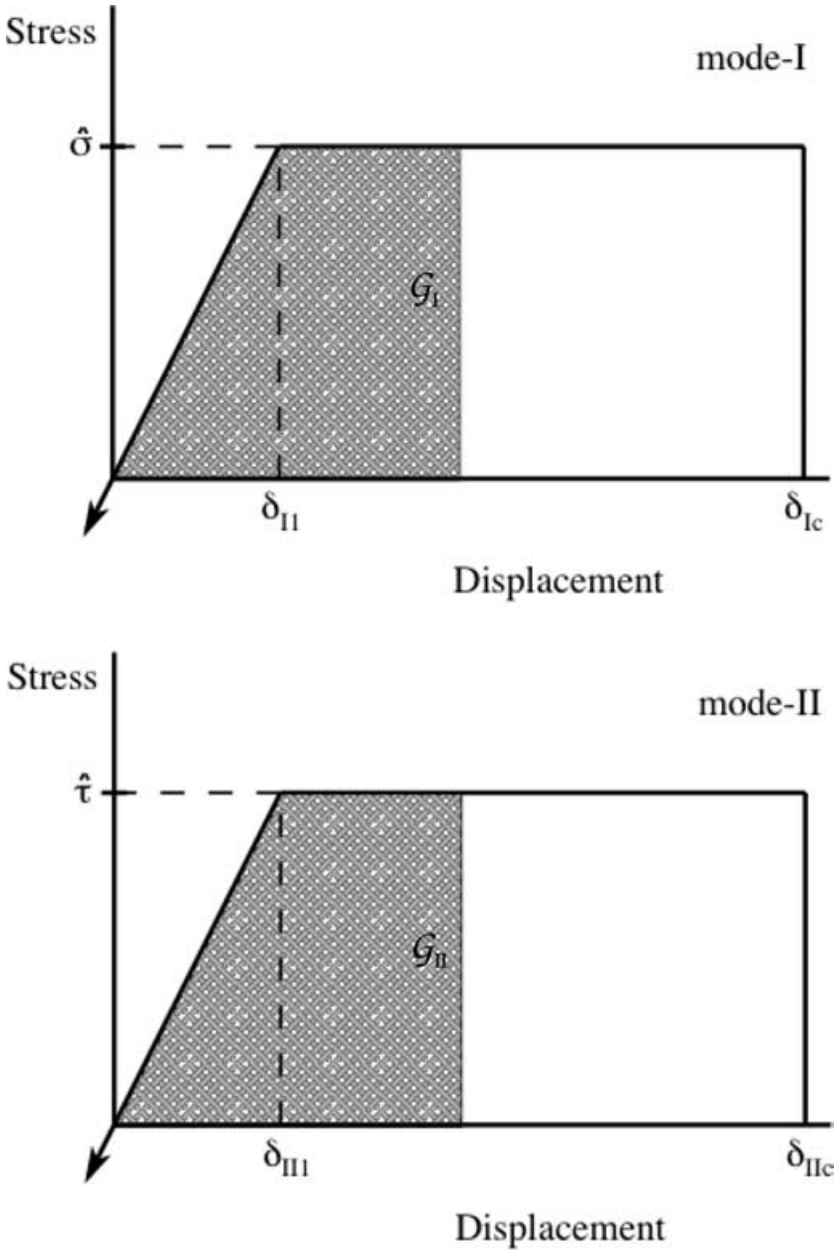

Fig. 1 The form of the mode-I and mode-II traction-separation laws used in this work. The mode-III curve is assumed to be identical to the mode-II curve. Total area under each curve is equal to the toughness for the appropriate mode, Γ_I, Γ_{II} or Γ_{III}. The appropriate energy-release rates, $\mathcal{G}_I$, $\mathcal{G}_{II}$ or $\mathcal{G}_{III}$, are defined as the areas under each curve up to the current displacement.

thermal-expansion mismatch during welding. To investigate possible effects of work hardening caused by indentation of the electrodes, several spot welds were sectioned at the midline of the weld nugget, and Vicker's micro-indentation hardness measurements were made on the sectioned face. The results (Fig. 2) show some evidence of strain hardening in the material directly surrounding the nugget, but the level was too small to require inclusion in the continuum elements of the finite-element model. Strain hardening that occurred during the preparation of the specimens as they were bent into shape was explicitly included in the numerical models by modifying the material properties of the elements in the bent regions (see Fig. 3a, for example). The appropriate degree of strain hardening was determined from continuum finite-element simulations of the bending process. The residual stresses caused by thermal expansion were not explicitly included in the analysis. To do so correctly would have required additional process modelling of the weld, which is beyond the scope of this particular project. However, some of the effects of possible residual stresses may be implicitly included in as much as they may affect the cohesive properties of the nugget and pullout regions.

The mechanical properties of the aluminium alloy were determined by tensile tests.[21] The yield stress, σ_Y, was 113 ± 3 MPa. The Young's modulus, E, was 69 ± 5 GPa,

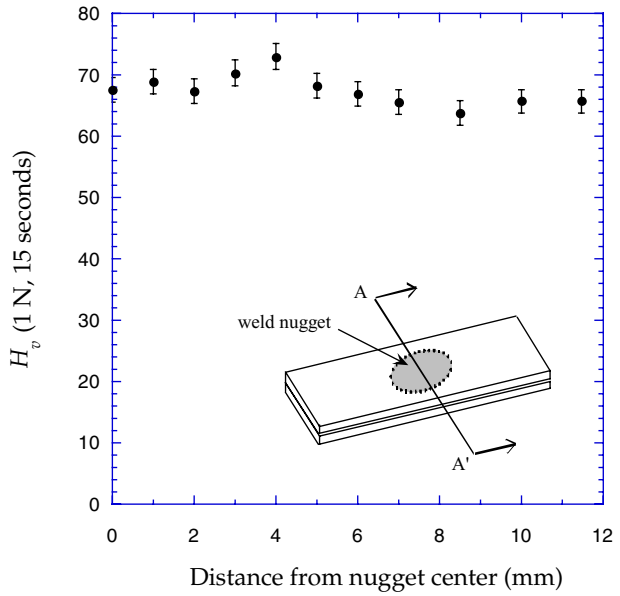

Fig. 2 Vicker's micro-indentation hardness as a function of distance from the nugget centre. This was obtained by sectioning spot-welded joints along the plane AA', polishing the resulting faces and conducting hardness measurements along the section. At a given distance from the weld centre, several hardness measurements were taken across the adherend thickness. The resulting average values are also shown.

and the true maximum stress was 289 ± 5 MPa. Poisson's ratio was taken to be 0.3. Post-yield data from the true stress–true strain curves of several tensile samples were fitted using the customary strain-hardening relation for true stress and strain of

$$\sigma = A\varepsilon^n \tag{2}$$

with $A = 494 \pm 6$ MPa and $n = 0.30 \pm 0.01$. These material properties were incorporated in the finite-element code to model the adherends, with further assumptions of isotropic hardening and a von Mises yield criterion.

Specimen preparation and testing

Coach-peel and lap-shear geometries were made by joining aluminium sheets with a single spot-weld (Fig. 3). The spot-welding was done using a mid-frequency, direct-current, spot-welding machine with electrodes in the shape of truncated cones with tip diameters of 8 mm. A square current waveform was used for all samples. Although slightly different weld schedules were used during the course of this study, it was assumed that these differences in weld schedules did not significantly affect the fracture parameters of the welds, and that properties determined from one set of welds could, with some acceptable level of approximation, be used for others. The size of the welds did, however, depend on the processing conditions and joint geometry, so that the diameters of the welds were measured and explicitly modelled in the numerical simulations. One set of coach-peel joints was fabricated using aluminium that was 1-mm thick, with a weld current of 25 kA for either 5 or 10 cycles at 60 Hz, producing nuggets with diameters in the range of 4.5–5.5 mm. Two further sets of coach-peel joints and two sets of lap-shear joints were fabricated using aluminium that was 2-mm thick. One set of each type of joint was made with a weld current of 17 kA for 15 cycles; this resulted in a weld diameter in the range of 4.25–5.25 mm. The other set of each type of joint was made with a weld current of 23 kA for 15 cycles; this resulted in large welds with diameters in the range of 6.5–7.5 mm.

The coach-peel specimens were tested in a screw-driven machine at a displacement rate of 5 mm per minute, with displacements between the points of load application being monitored optically using a C.C.D. camera. Failure of the 2.0-mm thick coach-peel joints always occurred within the nugget for the smaller set of welds, and it always occurred by pullout for the larger set of welds. The 1.0-mm thick coach-peel joints exhibited transitional behaviour with failure sometimes occurring as a combination of nugget fracture and pullout, and sometimes by pullout alone. The lap-shear specimens were tested in a screw-driven machine at a displacement rate of 0.5 mm per minute. Plastic deformation in the lap-shear joints was limited to plastic bending in the immediate region near the nugget. As a result, the deflections between the ends of the specimens were very small, and displacement measurements had to be focused on the nugget region. In particular, the relative displacement between two points in the plane of the centre-line of the nugget, on the edges of the two adherends closest to the nugget (see Fig. 3b), was measured using a C.C.D. camera. Failure of the 2-mm thick lap-shear specimens always occurred by nugget fracture for both larger and smaller welds.

Cohesive-zone properties of the nugget

Because the nugget always ruptured in the 2-mm thick specimens with the smaller welds, the coach-peel configuration of these specimens was used to deduce the mode-I cohesive-zone parameters for the nugget, and the lap-shear configuration was used to deduce the shear parameters.

Mode-I properties

The experimental load-displacement data for the 2-mm thick coach-peel geometry with the smaller welds (failing by nugget fracture) are shown in Fig. 4 by the dashed lines. Superimposed on Fig. 4 is a solid line representing the

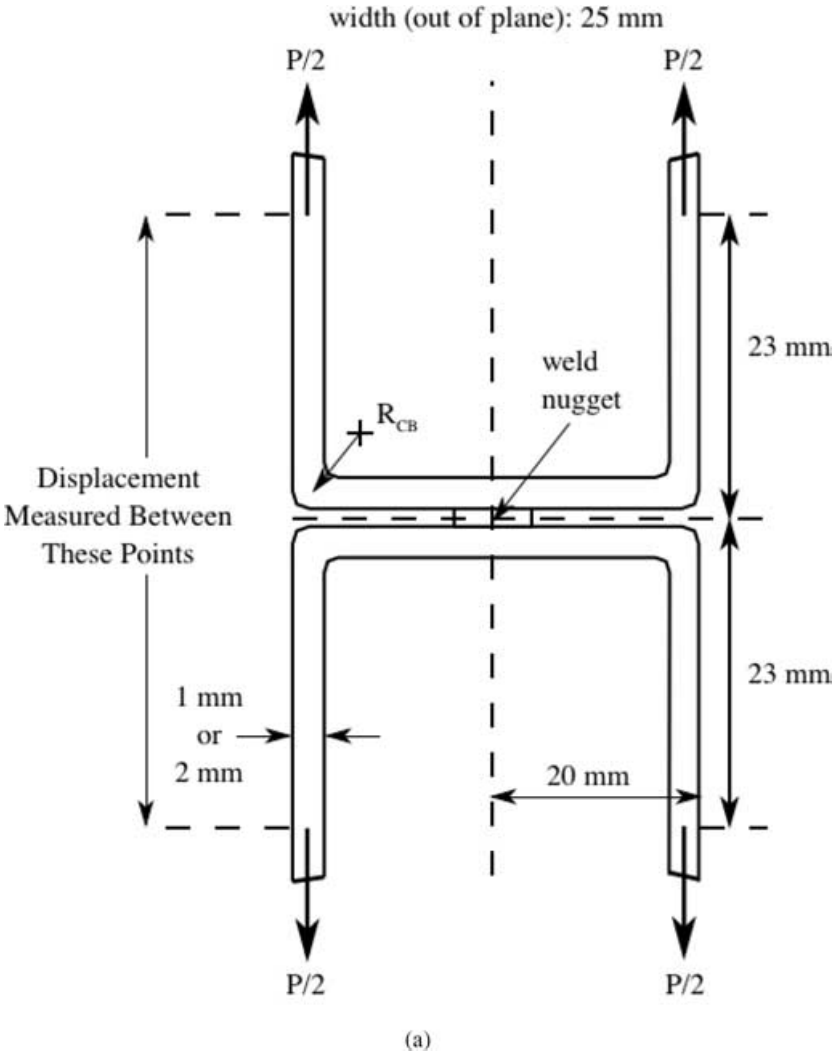

Fig. 3 Geometry and nominal dimensions of (a) the coach-peel specimens and (b) the lap-shear specimens used to determine the cohesive-zone parameters. The curvature R_{CB} for the coach-peel specimen was 2-mm for the 1-mm thick aluminium alloy, and 5 mm for the 2-mm thick alloy.

calculations of a cohesive-zone analysis that was determined to provide the best fit to the experimental data.[b] Because Fig. 2 indicates that there was very little change in hardness between the base metal and the weld nugget, consistent with a non-heat-treatable alloy, and observations of fractured weld nuggets showed few, if any, macroscopic voids, the mode-I cohesive strength of the nugget was chosen to be equal to the true maximum tensile strength of the alloy, 290 ± 30 MPa (with the increased uncertainty being associated with the uncertainty in the hardness measurements). Then, using this value of cohesive strength for the numerical calculations, the best fit between numerical results and the experimental load–displacement curves could be used to obtain a value of the mode-I toughness of the nugget. This was found to be given by $\Gamma_{IN} = 13 \pm 2$ kJm^{-2}. The effect of the quoted uncertainties for these parameters, as well as any uncertainties in the geometry of the experimental specimens, is indicated by error bars on the solid line in Fig. 4.

It should be noted that, had a simple strength-based failure criterion been used to fit the peak load supported by this geometry, an average cohesive strength for the nugget of about 125 MPa would have been obtained. It will be shown in a later section that such a simple approach overestimates the strength of another mode-I geometry by almost an order of magnitude. The introduction of toughness as a second cohesive parameter allows some progressive failure of the nugget to occur during deformation, and allows a more accurate prediction of the failure of the joint. Furthermore, while optical measurements of the displacements across the weld at failure had relatively large uncertainties, they were observed to be on the order of 0.05 to 0.1 mm, which compares very well with a critical

[b]In these calculations, fracture was only allowed to occur in the nugget region of the joint, so that complications associated with the possibility of alternative failure modes were avoided at this stage.

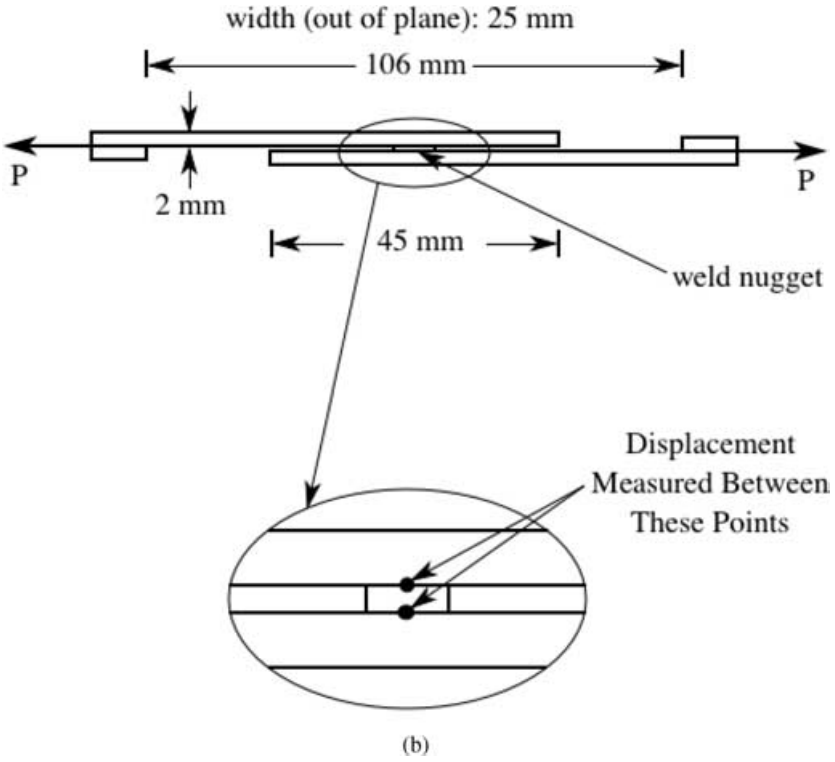

Fig. 3 Continued

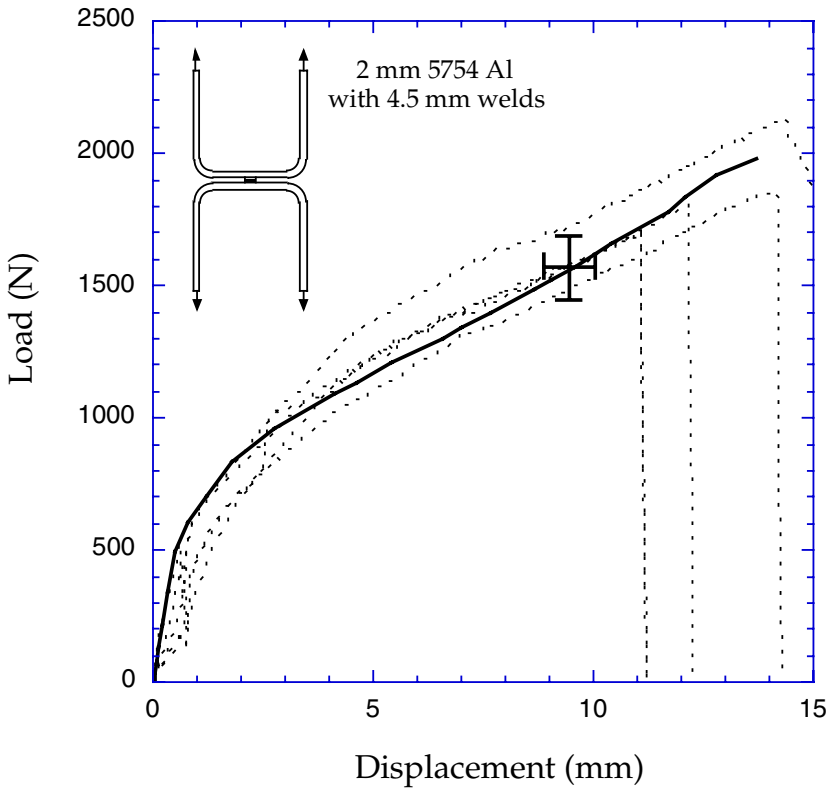

Fig. 4 A comparison between the numerical and experimental load-displacement curves used to deduce the mode-I cohesive parameters of the nugget from coach-peel specimens made from 2-mm thick 5754 aluminium with nugget diameters of approximately 4.5 mm. The uncertainty shown for the numerical curve arises from the variability of the geometry (including the size of the weld), the material properties of the aluminium and the range of cohesive parameters that gave reasonable agreement with the experimental results.

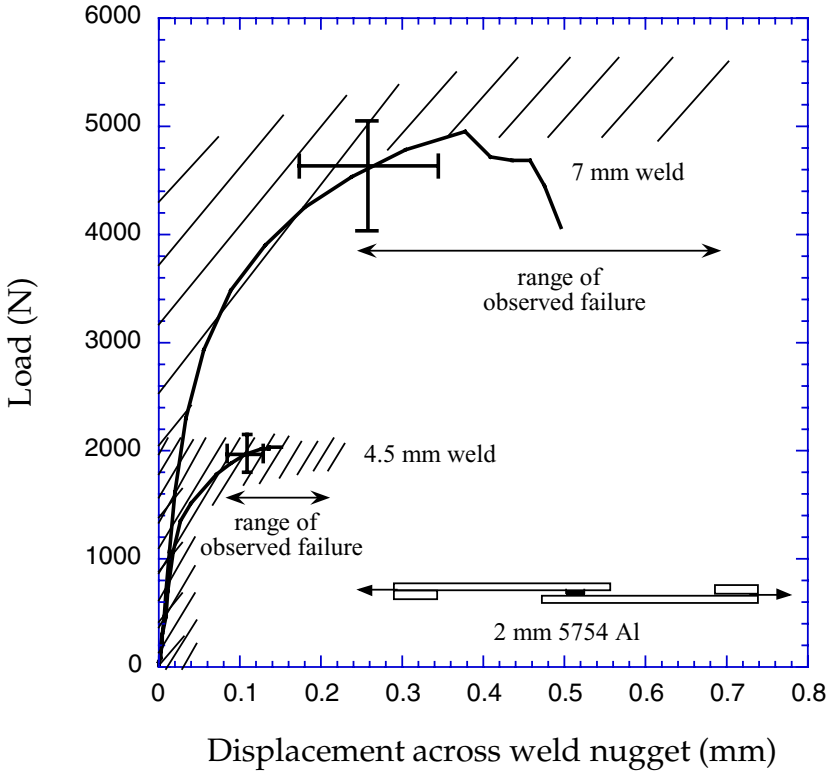

Fig. 5 A comparison between the numerical results and the range of experimental results for the load–displacement curves obtained from lap-shear specimens made from 2-mm 5754 aluminium with nugget diameters of approximately 4.5 mm and 7.0 mm. The displacement for both the experimental and numerical results is the relative displacement between the two points identified in Fig. 3b. In this figure, the numerical curve for the 4.5-mm nuggets is the result of fitting experimental data to deduce the mode-II cohesive parameters. These parameters were then used to predict the numerical curve for the 7.0 mm nuggets. Uncertainty in the experimental data was dominated by warping and rotation of the specimens during loading. The uncertainty shown for the numerical results indicates the effect of the variability of the geometry, including the size of the weld, the material properties of the aluminium and the cohesive parameters of the weld.

displacement of 0.08 mm that corresponds to the stated values of mode-I cohesive strength and toughness.

Mode-II properties

Nugget failure was always observed in the lap-shear specimens for both sizes of weld. The lap-shear is a mixed-mode geometry, so if the mode-I properties of the nugget are already known, the mixed-mode failure criterion (Eq. 2) can be used to deduce the mode-II cohesive-zone parameters from the experimental data.[12] Uncertainties in the experimental displacement data are large relative to the measured displacement values in the initial stages of these experiments because of warping and twisting of the specimens, coupled with the resolution of the C.C.D. images. As a result, any effects of changing parameters on the initial stiffness of the specimens could not be used for fitting. However, the final displacements and loads at which failure occurred were relatively consistent between specimens, and could be used for the purposes of deducing the mode-II parameters. Specifically, for fixed mode-I properties of the nugget, an increase in the mode-II cohesive strength increased the peak load and decreased the displacement at which catastrophic failure is observed (i.e. shifted the curve up and to the left), while an increase in the mode-II toughness increased the failure load slightly and greatly increased the failure displacement (i.e. shifted the curve up and to the right). These calculations indicated that the mode-II toughness for the nugget was $26 \pm 4\ \mathrm{kJm^{-2}}$, and the shear strength was 200 ± 20 MPa (lower set of data in Fig. 5).[c] It is interesting to note that the ratio between the mode-I and mode-II toughness values of the nugget (2.0 ± 0.7) obtained by this cohesive-zone analysis is consistent with those published by Banks-Sills *et al.*[22] and Cowie *et al.*[23] for aluminium alloys, and also that the ratio between the mode-I and mode-II nugget strengths (1.5 ± 0.3) obtained by this analysis is consistent with published data for a similar aluminium alloy.[24,25d] The mode-I and mode-II cohesive parameters were then used without modification to predict the behaviour of the specimens with larger welds (upper set of data in Fig. 5).

Cohesive-zone properties for pullout failure

Pullout failure was always observed in the 2-mm thick coach-peel samples with large welds, and it was observed in more than half of the 1-mm thick coach-peel specimens containing smaller welds. In the rest of these latter specimens, nugget fracture and weld pullout occurred simultaneously. No differences associated with failure mechanism could be detected in the load-displacement curves for

[c]Again, fracture was only allowed to occur in the nugget region of the joint for these initial numerical calculations.
[d]5454 aluminum.

these specimens, nor was there any correlation with the precise nugget size. Clearly, the range of material properties was such that this geometry exhibited a transition in the failure mechanism; this was subsequently confirmed when all the cohesive parameters had been determined.

Characterization of the cohesive parameters for pullout was complicated because the mode mixedness is a function of location around the nugget. This precluded isolation of the normal and shear properties, as was done for nugget failure. As a result, it was not possible to use a single geometry to determine one set of pullout parameters and another geometry to determine the other. The cohesive parameters had to be deduced by simultaneously investigating at least two geometries that exhibited pullout failure. This was done by using experimental data for the 2-mm coach-peel specimens with a weld size of 7.0 mm, and the 1-mm coach-peel specimens for which only pullout occurred. Two numerical models of each geometry were programmed, one which allowed only pullout failure, using continuum elements for the weld nugget and a second which allowed pullout failure and nugget fracture, using the mode-I properties for nugget fracture determined previously.

Owing to the geometrical differences between the 1-mm and 2-mm coach peel joints, the relative portions of bending and shearing stresses in the material which experiences pullout failure are not the same. Consequently, the behaviour of these two geometries appears to depend on the four cohesive-zone parameters in different ways. For the 1-mm thick coach-peel specimens, changes in the mode I cohesive strength, $\hat{\sigma}_P$, have the largest effect on the load and displacement at fracture. Changes in either $\hat{\tau}_P$ or Γ_{IIP} have a similar effect, but are less significant than changes in $\hat{\sigma}_P$. Changes in Γ_{IP} have very little effect in this geometry. In contrast, the relative order of importance for the cohesive parameters for pullout in the 2-mm thick coach-peel specimens was $\hat{\tau}_P$, $\hat{\sigma}_P$ and Γ_{IP} (both having similar effects), followed closely by Γ_{IIP}. Therefore, a relatively narrow range of pullout parameters could be obtained by first comparing the experimental results to numerical results of a model that only permitted nugget pullout, and then by confirming that these parameters predicted only pullout failure when the possibility of both nugget fracture and pullout were incorporated in the numerical models Following this procedure, the cohesive parameters for pullout of the nugget were determined to be $\hat{\sigma}_P = 340 \pm 10\,\text{MPa}$, $\hat{\tau}_P = 230 \pm 10\,\text{MPa}$, $\Gamma_{IP} = 13 \pm 2\,\text{kJm}^{-2}$ and $\Gamma_{IIP} = 26 \pm 4\,\text{kJm}^{-2}$. Figure 6 shows a comparison between the calculated load–displacement data (solid lines), based on these values of cohesive-zone parameters, and the observed load–displacement plots for the 1- and 2-mm thick

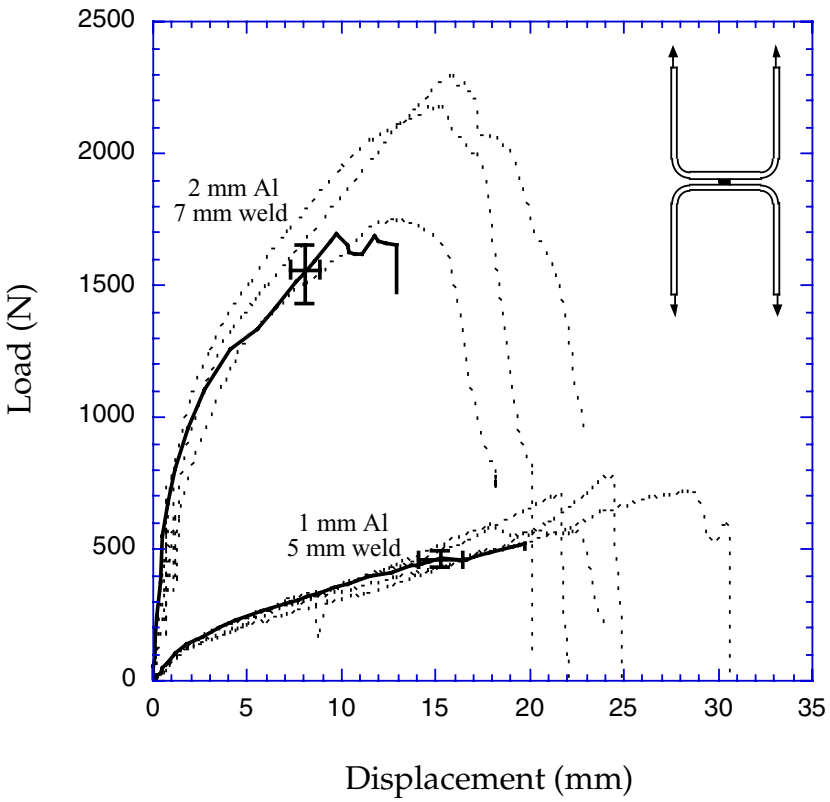

Fig. 6 A comparison between the numerical and experimental load–displacement curves used to deduce the pullout cohesive parameters from coach-peel specimens made from 1-mm thick 5754 aluminium with nugget diameters of approximately 5.0 mm, and 2-mm thick 5754 aluminium with nugget diameters of approximately 7.0 mm. The uncertainties shown for the numerical curves arise from the variability of the geometry (including the size of the weld), the material properties of the aluminium and the range of cohesive parameters that gave reasonable agreement with the experimental results.

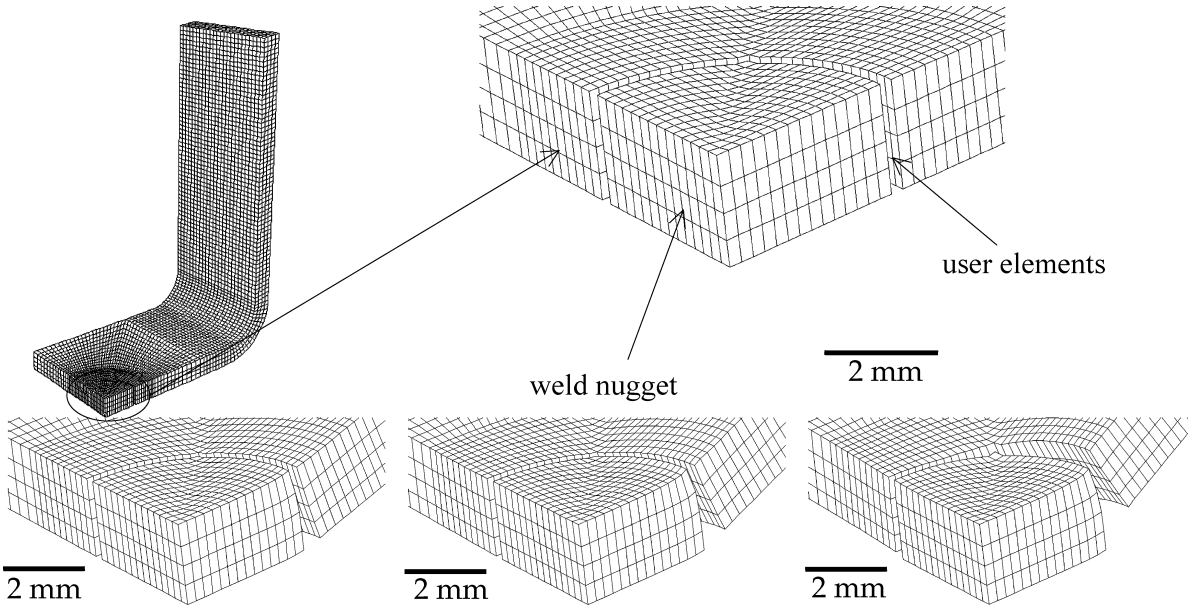

Fig. 7 The progression of pullout failure in a numerical model of a coach-peel joint. Fracture begins in a region dominated by mode-I loading. The mode-II and -III components increase (and the mode-I component decreases) as the crack progresses around the weld nugget.

coach-peel geometries that failed by pullout (dashed lines). In both cases, the strength and maximum displacement of the numerical models are near the lower end of the experimental range, but show reasonable agreement. It should be noted that, within the limits of a four-parameter model, better fits to the data were not found; fitting the peak load and displacements did not provide a satisfactory fit to the overall shape.

Figure 7 shows details of the numerical calculations of how pull out occurs, and illustrates the complicated mixed-mode nature of the problem with all three modes of deformation occurring simultaneously. This combined tearing and shearing appears to capture the actual mechanism quite well, but the numerical model was limited in that an eightfold symmetry was imposed for the coach-peel calculations, so that the effects of asymmetrical failure and nugget rotation seen in the actual specimens were not captured numerically. These issues of symmetry and rotation probably impaired the level of agreement that could be obtained between the numerical simulations and the experimental results.

MODEL VERIFICATION

Verification was done by exploring T-peel specimens containing either one or two spot welds, as shown in Fig. 8. Specimens with a single spot-weld were fabricated from 1-mm thick 5754 aluminium alloy sheets using a weld schedule of 25 kA for 10 cycles, resulting in a nugget diameter of 4.0 ± 0.25 mm. Additional specimens containing either one or two spot welds were fabricated from 2-mm thick 5754 aluminium alloy sheets using a weld schedule of 17 kA for 15 cycles, resulting in a nugget diameter of 4.0 ± 0.5 mm. It was observed that the weld nuggets in these specimens were slightly eccentric, and this eccentricity was incorporated in the numerical modelling. The numerical predictions for the load–displacement plots (with the displacement being measured between the points indicated in Fig. 8) are shown in Fig. 9. It should be emphasized that these predictions were obtained by using the cohesive parameters obtained in the previous section; no further modifications have been done. The numerical results indicated that the specimens made from the 2-mm thick aluminium fail by nugget fracture, whether they contained one or two welds; whereas, the failure of the 1-mm thick T-peel specimens is at the borderline between nugget fracture and pullout. The numerical results also indicated that the double-welded specimens fail in a sequential fashion, with a precipitous drop in load after the first weld fails.

The actual specimens were tested under displacement control at a rate of 5 mm per minute, and the displacements were measured between the points of load application (as indicated in Fig. 8). The experimental load–displacement curves have been plotted in Figs 10a and (b) as dotted lines, and the numerical predictions from Fig. 9 have been superimposed on these plots as solid lines. It should be noted that both the loads and displacements, and hence the energy dissipated during fracture, agree quite well with the numerical predictions. Furthermore, the observed failure modes were consistent with the numerical predictions: nugget fracture always occurred in

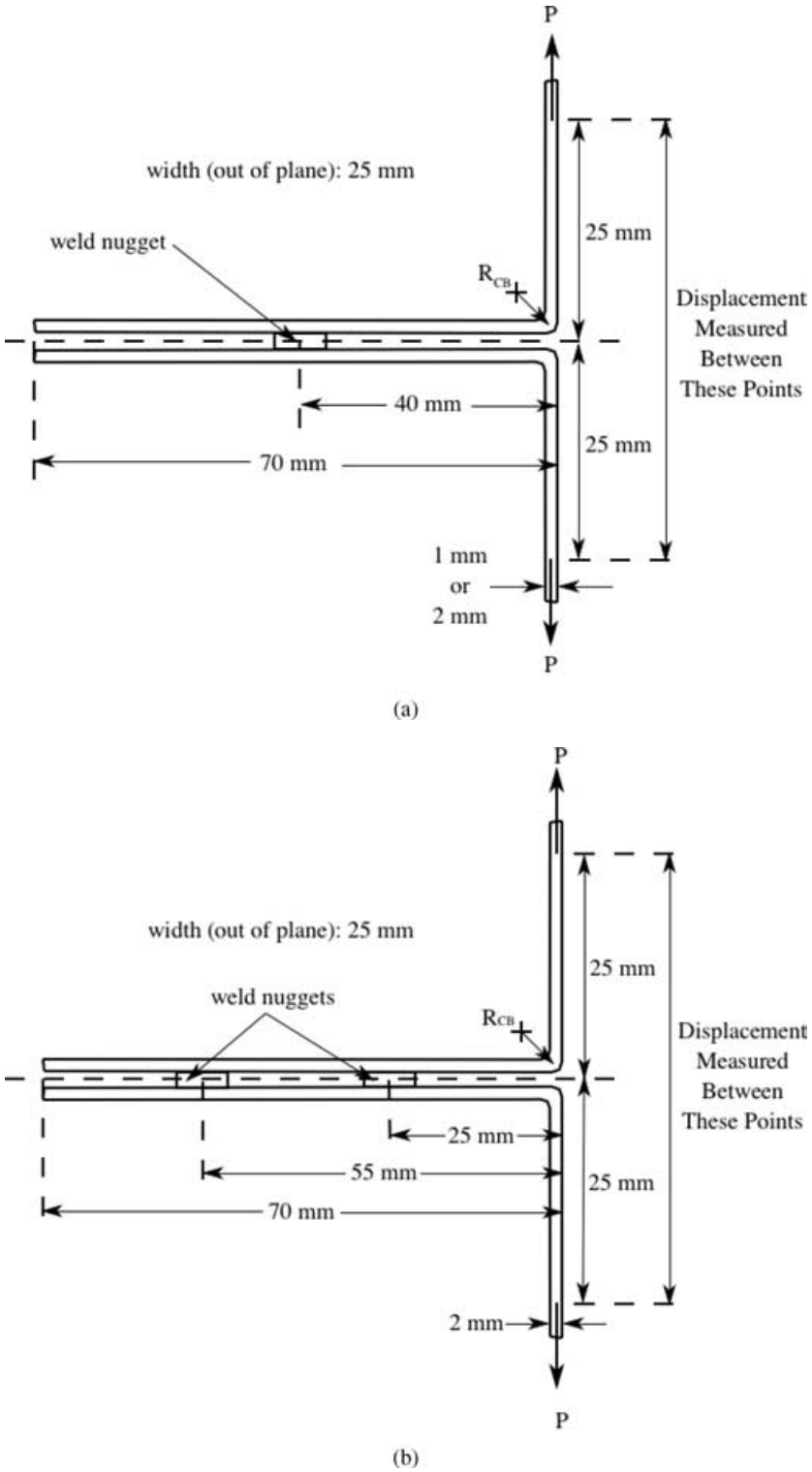

Fig. 8 Geometry and dimensions for the (a) T-peel specimens with 1 spot-weld and (b) T-peel specimens with two spot welds used to verify the cohesive-zone parameters. The curvature, R_{CB}, was 2-mm for the 1-mm thick aluminium alloy, and 5 mm for the 2-mm thick alloy.

the 2-mm thick specimens (whether they contained one or two welds), and a combination of nugget fracture and weld pullout occurred in the 1-mm thick specimens. All these results confirm that the cohesive parameters for the nugget and pullout region are correct, and indicate that a cohesive-zone approach has good potential for providing a predictive and quantitative approach for modelling the failure of spot-welded joints.

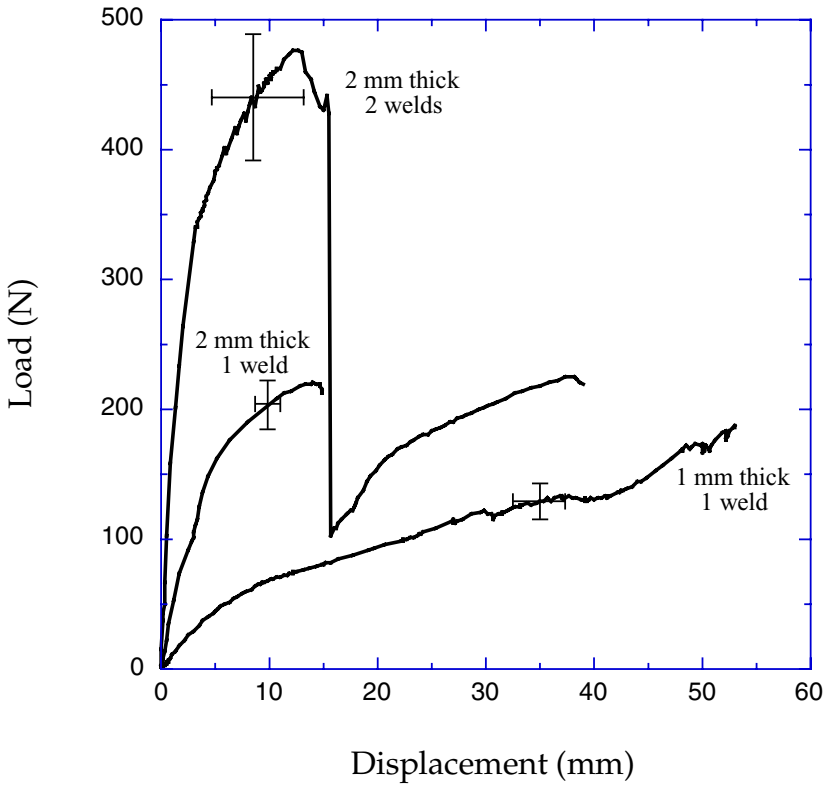

Fig. 9 Numerical predictions for the load–displacement curves obtained from the T-peel specimens described in Fig. 9 made from welds with diameters of 4 mm. The uncertainty shown for the numerical results indicates the effect of the variability of input parameters associated with the geometry, including the size of the weld, the material properties of the aluminium and the cohesive parameters of the weld.

To appreciate the power of this modelling method, and to dispel the notion that weld strength can be described in terms of an average strength, rather than in terms of the strength and energy criterion proposed in this paper, a comparison between Figs 4 and 10a is particularly instructive. From Fig. 4, it will be seen that the 2-mm thick coach-peel samples with an average nugget size of about 4.5 mm supported a peak load of about 2000 N. The use of these numbers with a simple strength criterion would result in an average nugget strength of approximately 125 MPa. If this nugget strength was then used to predict the load-carrying capacity of the 2-mm thick T-peel specimens of Fig. 10a (with a slightly smaller nugget size of 4 mm), a peak load of about 1600 N would be obtained. The actual load that the structure could carry was almost an order of magnitude lower than this, and was predicted very accurately by the cohesive model presented in this paper. This comparison between the two geometries emphasizes that even if a single strength parameter can describe the behaviour of a weld in one loading configuration, it cannot be used as a universally applicable parameter, even when the loading mode is nominally identical.

CONCLUSIONS

A numerical model for the failure of resistive spot welds based on a cohesive-zone analysis has been developed. The model uses two material parameters, a cohesive strength and toughness, for each possible mode of loading in each region of potential failure. While extracting the parameters from a welded configuration is not straightforward, it appears that, with some care, a range of suitable parameters can be determined that have a predictive capability. This has been demonstrated by exploring two geometries that have very different stress distributions (the coach peel and the T-peel)—the cohesive-zone model captures a very dramatic change in strength associated with this difference in stress distribution. A single-parameter, strength-based criterion could not have done so.

The results presented in this paper show that the model is capable of capturing not only the load and deformation response of spot-welded joints, but also the transitions between nugget fracture and nugget pullout. This explicit link between material properties, joint geometry and failure mechanism contrasts with the typical view that a weld must 'pull a nugget' (fail by pullout) to be acceptable.[26] Nugget failure does not indicate the presence of a substandard weld—it simply indicates that nugget fracture was the preferred crack path based on the interaction of the loading, geometry and fracture parameters of the joint. An excellent example of this can be seen by the fact that identical welds (7-mm diameter) in identical sheets (2-mm thick) failed by pullout when tested in the coach peel geometry and by nugget failure when tested in the

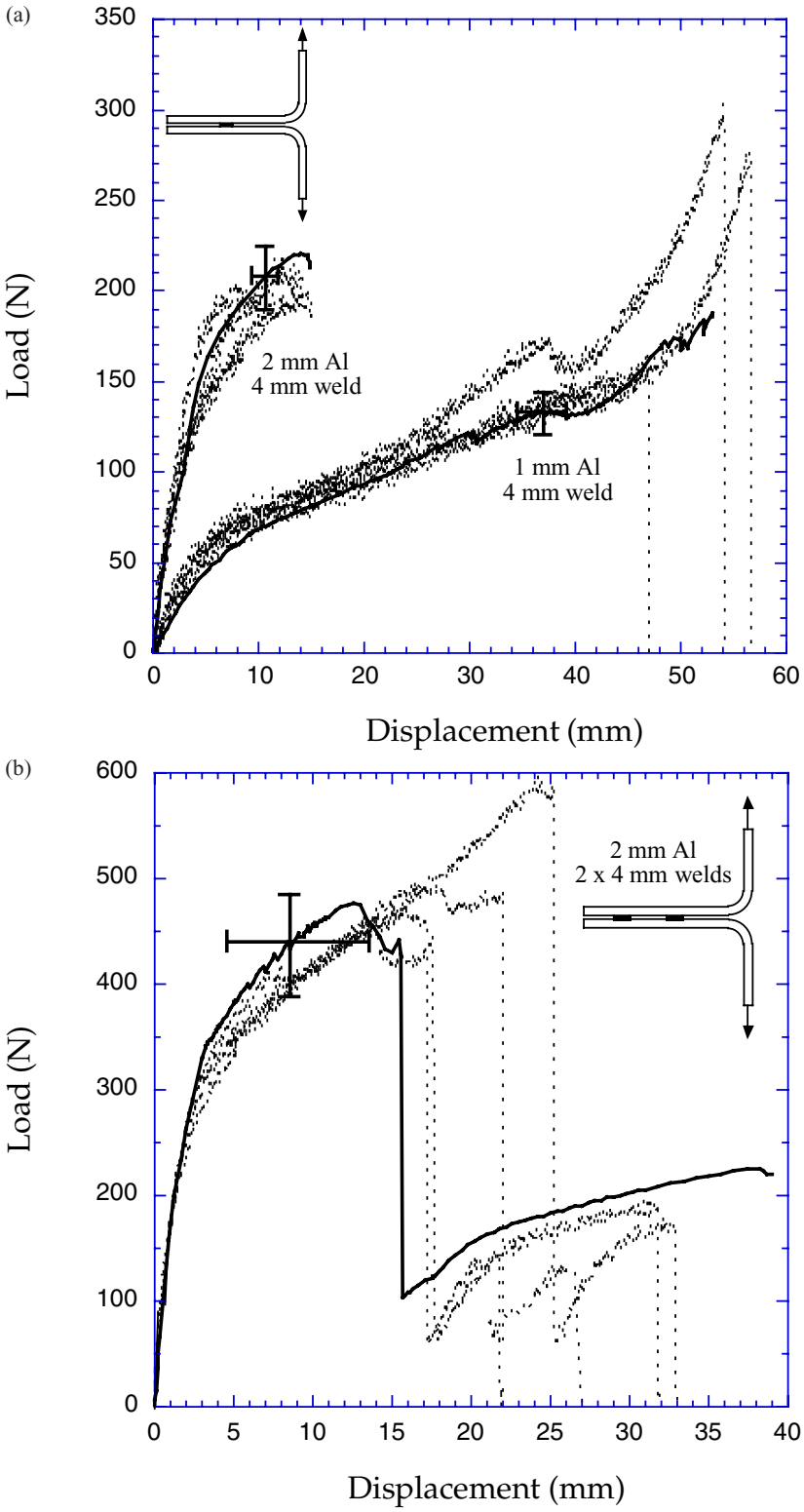

Fig. 10 Comparison between experimental results and the numerical predictions. **(a)** Load–displacement curves for a single spot-weld in a joint made from 1- and 2-mm thick aluminium. **(b)** Load–displacement curves for a specimen made with two spot welds and 2-mm thick aluminium.

lap shear geometry. Furthermore, the modelling clearly confirms that larger welds are more prone to failure by pullout, simply because the nugget area increases faster than the pullout area as the nugget diameter increases.

Acceptance of this more complete view of spot-weld fracture, together with the modelling approaches presented in this paper, will provide powerful tools for predicting the strength, deformation and energy absorption of

spot-welded joints. For example, a companion paper[27] has demonstrated how it is possible to use the cohesive-zone models for a spot-weld with the cohesive-zone model for an adhesive[8,11] to predict the behaviour of "weld-bonded" joints that combine adhesives and welds.

Acknowledgements

The authors would like to thank R. Cooper of Ford Motor Co., Scientific Research Labs (SRL), for help with the spot-welding machine as well as J. Hill, S. Ward and K. Lasarz, also of Ford SRL, for providing the 5754 aluminium and XD4601 adhesive. Helpful conversations with K. Garikipati of the University of Michigan are gratefully acknowledged. MNC was partially supported by the National Science Foundation through a Graduate Fellowship and through the American Welding Society through a Graduate Fellowship Research Grant.

REFERENCES

1 Satoh, T., Abe, H., Nishikawa, K. and Morita, M. (1991) On three-dimensional elastic-plastic stress analysis of spot-welded joint under tensile shear load. *Trans. Jpn Weld. Soc.* **22**, 46–51.
2 Chang, B. H., Shi, Y. W., Dong, S. J. (1999) Comparative studies on stresses in weldbonded, spot-welded and adhesive bonded joints. *J. Mater. Process. Technol.* **87**, 230–236.
3 Deng, X., Chen, W. and Shi, G. (2000) Three-dimensional finite element analysis of the mechanical behavior of spot-welds. *Finite Elem. Anal. Des.* **35**, 17–39.
4 Lee, Y. L., Wehner, T. J., Lu, M. W., Morrissett, T. W. and Pakalnins, E. (1998) Ultimate strength of resistance spot-welds subjected to combined tension and shear. *J. Test. Eval.* **26**, 213–219.
5 Lin, S. H., Pan, J., Wu, S. R., Tyan, T. and Wung, P. (2001) Failure loads of spot-welds under combined opening and shear static loading conditions. *Int. J. Solids Struct.* **39**, 19–39.
6 Wung, P. (2001) A force-based failure criterion for spot-weld design. *Exp. Mech.* **41**, 107–113.
7 Wung, P., Walsh, T., Ourchane, A., Stewart, W. and Jie, M. (2001) Failure of spot welds under in-plane static loading. *Exp. Mech.* **41**, 100–106.
8 Yang, Q. D., Thouless, M. D. and Ward, S. M. (1999) Numerical simulation of adhesively bonded beams failing with extensive plastic deformation. *J. Mech. Phys. Solids* **47**, 1337–1353.
9 Yang, Q. D., Thouless, M. D. and Ward, S. M. (2000) Analysis of the symmetrical 90°—Peel test with extensive plastic deformation. *J. Adhes.* **72**, 115–132.
10 Yang, Q. D., Thouless, M. D. and Ward, S. M. (2001) Elastic-plastic mode-II fracture of adhesive joints. *Int. J. Solids Struct.* **38**, 3251–3262.
11 Yang, Q. D. and Thouless, M. D. (2001) Mixed-mode fracture analysis of plastically deforming adhesive joints. *Int. J. Fract.* **110**, 175–187.
12 Kafkalidis, M. S. and Thouless, M. D. (2002) The effects of geometry and material properties on the fracture of single lap-shear joints. *Int. J. Solids Struct.* **39**, 4367–4383.
13 Needleman, A. (1987) A continuum model for void nucleation by inclusion debonding. *J. Appl. Mech.* **54**, 525–531.
14 Tvergaard, V. and Hutchinson, J. W. (1992) The relation between crack growth resistance and fracture process parameters in elastic-plastic solids. *J. Mech. Phys. Solids* **40**, 1377–1397.
15 Tvergaard, V. and Hutchinson, J. W. (1996) On the toughness of ductile adhesive joints. *J. Mech. Phys. Solids* **44**, 789–800.
16 Roychowdhury, S., Arun Roy, Y. D. and Dodds RH, Jr. (2002) Ductile tearing in thin aluminum panels: Experiments and analyses using large-displacement, 3-D surface cohesive elements. *Engng Fract. Mech.* **69**, 983–1002.
17 Cavalli, M. N. (2003) *Cohesive Zone Modeling of Structural Joint Failure*. Ph.D. Thesis, University of Michigan, Ann Arbor, USA.
18 Zuniga, S. M. and Sheppard, S. D. (1995) Determining the constitutive properties of the heat-affected zone in a resistance spot-weld. *Model. Simul. Mater. Sci. Engng* **3**, 391–416.
19 Bringas, H. E. (1999) *CASTI Metals Red Book, Nonferrous Metals*, 2nd ed. Edmonton, Alberta, Canada.
20 Sun, X. and Dong, P. (2000) Analysis of aluminum resistance spot-welding process using coupled finite element procedures. *Weld. J.* **79**, 215s–221s.
21 Standard E8M-99 (1999) *Standard Test Method for Tension Testing of Metallic Materials [Metric]*. American Society for Testing and Mateirals, USA.
22 Banks-Sills, L. D. and Sherman, D. (1991) *J*-II fracture testing of a plastically deforming material. *Int. J. Fract.* **50**, 15–26.
23 Cowie, J. G. and Tuler, F. R. (1991) Comparison of shear and tensile fracture in high strength aluminum alloys. *Int. J. Fract.* **47**, 229–239.
24 Davis, J. R., ed. (1994) *ASM Specialty Handbook: Aluminum and Aluminum Alloys*. ASM International, Material Park, USA, 680.
25 Holt, J. M. and Ho, C. Y., eds (1994) *Structural Alloys Handbook*. CINDAS/Purdue University, West Lafayette, USA.
26 Standard AWS C1.4M (1999) *Specification for Resistance Welding of Carbon and Low-Alloy Steels*. American Welding Society, USA.
27 Cavalli, M. N., Thouless, M. D. and Yang, Q. D. (2004) Cohesive-zone modeling of the deformation and fracture of weld-bonded joints. *Weld. J.* **83**, 133s–139s.